

1 **Projected Changes in the Seasonal Cycle of Surface Temperature**

2 JOHN G. DWYER *

Columbia University, Department of Applied Physics and Applied Mathematics, New York, NY

3 MICHELA BIASUTTI

Lamont-Doherty Earth Observatory, Columbia University, Palisades, NY

4 ADAM H. SOBEL

Department of Applied Physics and Applied Mathematics, Department of Earth and Environmental Sciences, and

Lamont-Doherty Earth Observatory, Columbia University, New York, NY

* *Corresponding author address:* John G. Dwyer, Department of Applied Physics and Applied Mathematics, Columbia University, 500 W. 120th St., New York, NY 10027.

E-mail: jgd2102@columbia.edu

ABSTRACT

6 When forced with increasing greenhouse gases, global climate models project a delay in the
7 phase and a reduction in the amplitude of the seasonal cycle of surface temperature, expressed
8 as later minimum and maximum annual temperatures and greater warming in winter than
9 summer. All 24 CMIP3 models agree on these changes and, over the 21st century, average
10 a phase delay of 5 days and an amplitude decrease of 5% for the global mean ocean surface
11 temperature. Most of the global mean changes come from the high latitudes, especially over
12 ocean. We provide evidence that the changes are mainly driven by sea ice loss: as sea ice
13 melts during the 21st century, the previously unexposed open ocean increases the effective
14 heat capacity of the surface layer, slowing and damping the temperature response. From the
15 tropics to the midlatitudes, changes in phase and amplitude are smaller and less spatially
16 uniform than near the poles, but they are still robust. These regions experience a small
17 phase delay, but an amplitude increase of the surface temperature cycle, a combination that
18 is inconsistent with changes to the effective heat capacity of the system. We propose that
19 changes in this region are controlled by changes in surface heat fluxes.

1. Introduction

On annual and longer time scales the seasonal cycle is responsible for around 90% of the total surface temperature variance. In this study we focus on potential changes in the seasonality of the surface temperature due to expected increases in greenhouse gases. These are distinct from changes due to the mean temperature increase, even though the latter can also affect the seasonality of climate-sensitive phenomena if they are linked to specific thresholds, such as streamflow timing due to melting snow (Stewart et al. 2005) and plant flowering (Fitter and Fitter 2002). Here we concentrate on changes to the phase and amplitude of the annual cycle in surface temperature (and to a lesser extent, temperature in the upper atmosphere), independent of the annual mean warming. Specifically, we are interested in the geographic pattern of the response in phase and amplitude to greenhouse gases and the mechanisms responsible for these changes.

In the models of the World Climate Research Programme’s (WCRP’s) Coupled Model Intercomparison Project phase 3 (CMIP3) multi-model dataset (Meehl et al. 2007), the main changes in the seasonality of surface temperature are a robust delay in phase and a robust decrease in amplitude. This means that the models predict peak temperatures to occur later in the year and the difference between annual maximum and minimum to shrink. We illustrate these effects in Figure 1 by plotting the hemispheric, multi-model mean 2 m surface air temperature over ocean for the last two decades of the 20th and 21st centuries with the annual mean removed. By fitting the anomalies to sinusoids we can quantify the changes compared to the late 20th century: the temperature cycle in the late 21st century has a phase delay of 6 days in the NH and 3 days in the SH and an amplitude decrease of 6% in the NH and 3% in the SH.

As we will show in Section 4, the dominant component of the global mean response is a strong phase delay and amplitude reduction over high-latitude ocean. Manabe and Stouffer (1980), Manabe et al. (1992), and Mann and Park (1996) noticed this high-latitude signal in earlier generations of climate models and proposed that it was a consequence of an increase in

47 effective heat capacity due to sea ice loss. Sufficiently thick sea ice insulates the atmosphere
48 from the ocean and curtails heat storage in the climate system. As the ice thins and melts,
49 the insulation weakens and disappears and the effective heat capacity of the surface increases.
50 Due to this additional thermal inertia, the temperature responds more slowly and with a
51 smaller amplitude than it would were the ice present.

52 We build on the earlier modeling studies by demonstrating the seasonality changes in the
53 most recent generation of climate models, investigating the spatial patterns of seasonality
54 changes, and providing substantial evidence that sea ice is driving the high-latitude season-
55 ality changes in the models. In order to verify this mechanism, we interpret the CMIP3
56 results in the context of a simple energy balance model for surface temperature. Using this
57 and other tools we show that the high-latitude phase delay and amplitude reduction are
58 consistent with an increased effective heat capacity and inconsistent with other potential
59 mechanisms including changes in the seasonality of surface heat fluxes or heat transport.
60 Furthermore, we link the effective heat capacity changes to sea ice loss quantitatively.

61 Previous observational studies in the NH midlatitudes found a phase advance driven
62 by changes over land and an amplitude reduction during the second half of the 20th cen-
63 tury (Thomson 1995; Mann and Park 1996; Stine et al. 2009) and have questioned the ability
64 of the CMIP3 models to reproduce the observed phase and amplitude variations. More recent
65 work by the same authors suggest that the small seasonality changes over land might be due
66 to natural variability in atmospheric circulation (Stine and Huybers 2012). The same study
67 also finds a non-statistically significant phase delay and an amplitude reduction in the NH
68 midlatitudinal oceans. Other recent studies of surface temperature over the Arctic Ocean
69 also found evidence of a phase delay and amplitude decrease due to strong late fall and
70 early winter warming during the last 20–30 years (Serreze et al. 2009; Screen and Simmonds
71 2010). Since the projected changes in seasonality do not become large until well into the 21st
72 century, we do not necessarily expect them to agree with observations for the 20th century.
73 Yet the correspondence between Arctic sea ice loss over the last few decades (Stroeve et al.

74 2007) and local changes in seasonality suggests that a key mechanism for the simulated late
75 21st century seasonality changes is also present in nature, irrespective of the inability of
76 models to reproduce observed trends over land.

77 At lower latitudes there is a smaller, yet still robust change in the temperature seasonality
78 that is different in nature from the high-latitude signal. Although small, these temperature
79 changes might be linked to seasonality changes in the onset and demise of the monsoons (Bi-
80 asutti and Sobel 2009; Seth et al. 2011), especially given the sensitivity of the Intertropical
81 Convergence Zone to the tropical sea surface temperature distribution (for example, Chiang
82 et al. (2002)). In the tropics and subtropics, the CMIP3 models project a small phase delay
83 and an amplitude increase, the latter being opposite in sign to the high-latitude amplitude
84 response. Because the phase and amplitude changes are of the same sign, these low-latitude
85 changes cannot be primarily driven by a change in effective heat capacity. Instead, some
86 other effect must be the primary cause. We provide evidence that changes in the seasonality
87 of surface flux are linked to the low-latitude temperature phase delay and amplitude increase.
88 The source of the low latitude changes in fluxes is not clear, but it might be linked to wind
89 speed changes as explained in Sobel and Camargo (2011)

90 The rest of the paper is laid out as follows. In the next section we give background
91 information on the data we analyze from CMIP3 and a reanalysis dataset and explain the
92 methods we use to calculate the phase and amplitude of the annual cycle. In Section 3
93 we describe the climatological structure of the annual cycle at the surface and aloft as
94 represented by both the CMIP3 multi-model mean and the reanalysis and demonstrate
95 agreement between the two, as both capture the slow, weak surface temperature response to
96 insolation over ocean and the fast, strong response over land. Moreover both datasets show
97 that over sea ice, the temperature response is more land-like than ocean-like. In Section 4
98 we detail the changes to the annual cycle at the surface and aloft as projected by the models
99 and discuss the differences at high and low latitudes. In Section 5 we look at both of
100 these regions individually and demonstrate that the changes in sea ice account for much of

101 the high-latitude temperature cycle change, while changes in the seasonality of surface flux
102 explain the seasonal temperature changes. Finally, we summarize our findings in Section 6.

103 **2. Data and Methods**

104 Throughout this study we use the CMIP3 20th century historical simulations (20C3M)
105 and 21st century A1B scenario simulations, where CO₂ emissions peak in the middle of
106 the 21st century and decrease thereafter (Meehl et al. 2007). Monthly temperature data
107 is sufficient to characterize the phase and amplitude of the annual cycle. We only use one
108 realization of each model. All 24 models store temperature data at all levels, but only 20
109 models store sea ice data and 18 store total surface flux data. When data is missing, we take
110 the multi-model mean to be the subset of models with available data. Surface temperature
111 is defined as 2 m air temperature, which is linked to SST over open ocean, though not over
112 sea ice (since SST is constrained to the melting point of sea water). To compare the model
113 results with observations, we use the European Centre for Medium-Range Weather Forecasts
114 (ECMWF) ERA-40 reanalysis data set (Uppala et al. 2005), which covers 1958–2001.

115 We calculate the phase of the seasonal cycle using two different techniques. The first uses
116 empirical orthogonal functions (EOFs). In this approach we decompose the climatological
117 mean, monthly data into spatial eigenfunctions of the covariance matrix and associated
118 principal component time series (PCs) (Kutzbach 1967). We obtain amplitude and phase
119 information by fitting a sinusoid to the principal component representing the annual cycle,
120 which is always associated with the EOF capturing the highest fraction of the total variance,
121 except within about 5° of the equator. The other method is Fourier transforming the data to
122 obtain the annual harmonic of each field of interest. Both methods are able to resolve phase
123 and amplitude precisely from monthly data. Fourier transforms can be calculated pointwise,
124 but they cannot obtain reliable phase information in the tropics because of the relatively
125 small amplitude of the annual cycle there. EOFs are defined for the entirety of the domain

126 of interest, but are dominated by regions of large annual variance. After spatially averaging
127 area-weighted phases and amplitudes calculated with a Fourier transform, the results are
128 nearly identical to those calculated using EOFs over the same domain.

129 Since our analysis is predicated on the temperature cycle being accurately described by a
130 sinusoid with a period of one year, we will only use locations for which the annual component
131 explains at least 80% of the total variance. These are roughly the same regions for which
132 insolation is dominated by the annual harmonic (Trenberth 1983). Surface temperature and
133 insolation each have over 95% of their total variance described by the annual cycle between
134 20° and 70°. At higher latitudes only around 85% of the insolation is due to the annual cycle
135 due to the sunless winters and nightless summers, but the annual cycle is still dominant
136 enough that we include these regions in our analysis. Over Antarctica, the temperature
137 cycle has a large semi-annual component due to the “coreless winters” of relatively constant
138 cold temperatures owing to the large landmass being in longwave radiative balance as well
139 as to dynamical effects (Loon 1967). In the Arctic, the temperature cycle is surprisingly
140 annual, with over 95% of the total temperature variance described by the first harmonic.
141 The strength of the annual harmonic of temperature in the Arctic can be partly attributed
142 to the seasonal sea ice cycle, which is not discrete, but instead smoothly varies throughout
143 the year with advancing and retreating ice margins, thickening and thinning sheet ice, melt
144 pond formation and other effects (Eicken 2008). In the tropics, the second harmonic becomes
145 prominent since the sun passes overhead two times per year. The variance explained by the
146 annual insolation and temperature cycle drops sharply into the deep tropics, and within 10°
147 of the equator less than 85% of the total variance is due to the annual cycle.

148 The Earth’s axial and apsidal precession also changes the phase of the temperature cycle
149 towards earlier seasons in the NH and later seasons in the SH (Stine and Huybers 2012).
150 Only four of the CMIP3 models have a different phase of insolation between the 20th and
151 21st centuries. We account for any such changes by measuring the temperature phase relative
152 to the local insolation phase, so that any phase changes in the models are not due to celestial

153 mechanisms.

154 **3. Climatological Structure**

155 Before analyzing the changes to the annual cycle, we look at the long-term mean of the
156 phase and amplitude at the surface and aloft for both models and the reanalysis. Most
157 models are clustered within about 5 days of the multi-model mean phase and about 15% of
158 the mean amplitude (though in any given year, there is a 15-20 day phase difference and
159 nearly a factor of two difference in amplitude between the most extreme models as in Figure 5
160 in Section 4). Despite the presence of several models with large biases, the multi-model mean
161 is representative of most models.

162 *a. Surface*

163 The seasonality of incoming diurnal mean solar radiation depends only upon latitude.
164 The phase of annual insolation is a weak function of latitude varying by only a few days
165 between the tropics and poles, but the amplitude of annual insolation increases markedly with
166 latitude from about 50 W m^{-2} at 10° to around 275 W m^{-2} at 90° (Trenberth 1983). Since the
167 temperature cycle is primarily governed by the solar cycle, the seasonality of temperature has
168 a pattern that is qualitatively similar to that of insolation, but with substantial departures
169 due to the local effective heat capacity of the surface layer.

170 Effective heat capacity of the surface is a function of both the material properties and
171 dynamical behavior of the layer adjacent to the atmosphere. We refer to it as effective since
172 it is neither the intensive heat capacity (per unit mass) of some material substance, nor the
173 extensive heat capacity of a fixed mass of that substance. Rather, it is the heat capacity of the
174 layer of material through which heat is transported sufficiently rapidly that it is influenced
175 by the atmosphere on time scales of interest. The mixed-layer ocean has a relatively large
176 heat capacity because turbulent mixing in it is effective in transporting heat downward so

177 that a thick layer of water is rapidly influenced by air-sea heat exchanged. This causes ocean
178 surface temperature to respond sluggishly and with small amplitude to heat fluxes at the
179 ocean surface. Temperature has a much faster and stronger response to insolation over land
180 than ocean because only a very thin layer of the land responds on annual time scales, since
181 the primary soil heat transfer process is diffusion with a small diffusivity. The effective heat
182 capacity of land depends to some extent on the type of soil and the moisture content, but a
183 typical estimate would be equivalent to a 6 m ocean mixed layer depth (Carson and Moses
184 1963). For comparison, the heat capacity of a tropospheric air column is roughly equivalent
185 to that of 4 m of ocean.

186 We plot the ERA-40 reanalysis and CMIP3 multi-model mean surface temperature phase
187 lag from insolation averaged over 1958–2001 in Figure 2(a) and 2(b), respectively. The
188 models show good fidelity to observations in their geographic structure. Phase delays are
189 smaller over the continents, as temperature over land responds more quickly than over ocean,
190 and this effect is propagated downwind (the temperature phase in the NH midlatitudes can
191 be well described by the westward distance from the coast (Stine et al. 2009)). The largest
192 differences between models and observations are mainly over the midlatitude oceans where
193 the models have a larger phase lag than those of observations (Figure 2(c)).

194 In regions of sea ice (e.g., the high-latitude Arctic and Southern oceans), the phase lag
195 has a response in-between those of land and ocean. Around the maximal winter extent ice
196 margins, the temperature responds slowly - as over the ocean - while closer to the poles the
197 temperature response is more akin to land for both observations and models. This pattern is
198 consistent with the insulating effect of sea ice becoming stronger in regions of more extensive
199 and thicker ice coverage, and being responsible for the rapid polar temperature response due
200 to a reduced effective heat capacity.

201 A similar pattern holds for the amplitude. Figure 2(d) and 2(e) show the temperature
202 amplitude from the ERA-40 reanalysis and the CMIP3 multi-model mean, respectively. Both
203 show that most of the surface has a relatively weak seasonal cycle with an amplitude under

204 5°C. The cycle is much stronger over land and sea ice, though. The difference between
205 models and observations is plotted in Figure 2(f). Differences are mostly small, though the
206 models are biased towards a larger amplitude in most places.

207 We provide more evidence that effective heat capacity sets the climatological surface
208 temperature phase and amplitude and that the ice-covered ocean has a similar heat capacity
209 to land in Figure 3. In both Figure 3(a) and (b) we plot the percentages of land and sea ice
210 that comprise each zonal band as a function of latitude. In Figure 3(a) we plot zonal mean
211 temperature phase, while in Figure 3(b) we plot zonal mean temperature amplitude divided
212 by insolation amplitude. The phase is strongly anti-correlated with the fraction of land and
213 sea ice ($r = -0.90$), while the amplitude is strongly correlated ($r = 0.82$), as we expect from
214 the different effective heat capacities of ocean and land or sea ice. If sea ice is not included,
215 correlations of land fraction drop to $r = -0.63$ with phase and $r = 0.62$ with amplitude,
216 indicating that ice-covered ocean has a land-like effective heat capacity.

217 *b. Aloft*

218 The zonal mean temperature phase aloft as a function of latitude and pressure is plot-
219 ted in Figure 4(a) and (b) for the ERA-40 reanalysis and the CMIP3 multi-model mean,
220 respectively. While the two exhibit some differences, they have similar overall structures.
221 For much of the troposphere, the phase lag stays roughly constant with height above the
222 boundary layer, presumably reflecting vertical mixing from the surface. Figure 4(c) shows
223 the difference in phase lag between models and observations. Most locations differ by less
224 than 5 days.

225 Figure 4(d) and (e) show the corresponding plots for the amplitude. Both observations
226 and models have a very different amplitude structure between the NH and SH. The high-
227 latitude NH has an amplitude that falls off with height, while in the SH the amplitude is
228 more vertically coherent and less variable overall. One difference between these two regions
229 is the amount of land. Land comprises most of each latitude band poleward of 45°N while

230 elsewhere it is mostly ocean (ignoring Antarctica) as in Figure 3. Observations and models
231 agree well on these features as shown in Figure 4(f).

232 4. Projected Changes

233 Beginning around the second half of the 20th century and continuing through the 21st
234 century, the models simulate a roughly linear increase in the global mean surface temperature
235 phase lag from insolation and a linear decrease in the amplitude. These global changes are
236 present for each of the 24 CMIP3 models in the time-series of phase (Figure 5(a)) and
237 amplitude (Figure 5(b)). The changes over land are smaller and less robust than those
238 changes over ocean, consistent with the idea that sea ice loss is driving much of the change.
239 The interannual variability of both the phase and amplitude over ocean is smaller than the
240 changes in these quantities over the 21st century.

241 *a. Surface*

242 Where a change in effective heat capacity is the dominant mechanism altering the annual
243 cycle of surface temperature, changes in phase and amplitude are constrained to be of the
244 opposite sign. For example, if the effective heat capacity increases, the phase will shift to
245 later in the year and the amplitude will decrease. On the other hand, in any region where
246 there are changes in phase and amplitude which are not of opposite sign, changes in effective
247 heat capacity are most likely not the primary driver.

248 The projected annual cycle changes in the 21st century are consistent with an effective
249 heat capacity increase in regions of large climatological sea ice cover. Figure 6(a) and (b)
250 show latitude-longitude maps of the multi-model mean projected temperature phase and
251 amplitude changes between the last two decades of the 21st century and the last two decades
252 of the 20th century. The largest changes are over high-latitude ocean with prominent sea ice,
253 including the entire Arctic Ocean and the Weddell and Ross Seas of Antarctica. Changes

254 in these regions are robust: at least 75% of models agree with the multi-model mean on the
255 sign of these changes (as indicated by the stippling).

256 Near the poles, the phase delay and amplitude decrease are much larger over ocean than
257 land. For example the delays in Greenland, Northern Canada, and the Antarctic coast are
258 all smaller than delays over ocean at the same latitude. The same holds true for amplitude,
259 as we would expect from an effective heat capacity increase over ocean. The largest changes
260 over high-latitude land are near the coast and fall off farther inland.

261 The phase delay in the tropics and subtropics is much smaller than at high latitudes,
262 and there are actually several regions of phase advance. There is no discernible land-sea
263 contrast in the low and midlatitudes suggesting that the homogenous delay is not solely due
264 to ocean heat capacity. Contrary to the phase change pattern, amplitude changes in the
265 subtropics show a clear large-scale change that is in the opposite direction from the high
266 latitudes: there is an amplitude increase of around 5% equatorward of 45° , most pronounced
267 over ocean regions. This amplitude increase is not as large as the polar amplitude decrease,
268 even after weighting by area. Yet this increase is robust among the models, especially in the
269 NH. In the deep tropics, where the semi-annual harmonic captures a large share of the total
270 variance, the amplitude of the second harmonic also increases by 15–20%, with the largest
271 changes in the Western Pacific Ocean. In between the low and high latitude responses
272 (around 45° - 60° in each hemisphere) is a transition zone where the amplitude change is
273 small. In any individual model, the region of change is smaller, but averaging over all of the
274 models enlarges it.

275 *b. Aloft*

276 The polar phase and amplitude changes are largest near the surface and weaken aloft,
277 as shown in Figure 7(a) and (b). This is what we would expect for annual cycle changes
278 controlled by surface characteristics, and supports the idea that the surface temperature
279 phase delay and amplitude reduction at the high latitudes are caused by an increased effective

280 surface heat capacity rather than dynamical changes aloft. The polar changes are likely
281 limited to the lower atmosphere because of the lack of deep vertical mixing due to the strong
282 local atmospheric stability, but we note that while the large surface phase delays are confined
283 to the boundary layer and do not extend above 850 hPa, the amplitude reduction extends
284 to around 600 hPa.

285 Away from the polar surface, most of the troposphere shows a small phase delay of one to
286 two days in the temperature cycle, of the same sign and similar in strength to the mean phase
287 changes at the midlatitudinal surface. Even though this delay is small, it is robust throughout
288 the high-latitude NH troposphere. In the subtropical midtroposphere, there are amplitude
289 decreases in both hemispheres seemingly independent from changes at the surface. Aside
290 from these regions, the rest of the troposphere has an amplitude increase, which is stronger
291 still in the midlatitude stratosphere (both in relative and absolute magnitude). Donohoe
292 and Battisti (2012) claim that this amplitude increase is due to an increase in absorbed
293 shortwave radiation by the atmosphere in the summer mainly because of increased water
294 vapor. There is an impressive amount of symmetry in the amplitude changes, considering
295 that the climatological amplitude is not that symmetric. The changes are also robust in
296 most locations, with exceptions mostly in regions near where the sign of the multi-model
297 mean change reverses.

298 **5. Mechanisms**

299 In response to increasing CO₂, the CMIP3 models show two different types of seasonal
300 temperature response. At high latitudes poleward of 60°, the CMIP3 models project a large,
301 robust phase delay and amplitude decrease, while at low latitudes equatorward of 45° there
302 is a smaller, less widespread phase delay and an amplitude increase. In a qualitative sense,
303 the changes at high latitudes are consistent with an increase in effective heat capacity caused
304 by reduced sea ice, while the low-latitude changes are not.

305 To understand these changes in a more quantitative manner, we find it useful to analyze
306 them in terms of a very simple model of the basic energy balance at the surface:

$$C \frac{dT}{dt} = F(t, T(t)), \quad (1)$$

307 where C is the effective heat capacity, T is the temperature, and F is the net heat flux
308 flux into the surface. Even though C has a seasonal dependence due to changing mixed
309 layer depths, sea ice, soil moisture and other effects, we treat it as a constant for each time
310 period. This is both for the sake of simplicity and because the results of interest prove
311 insensitive to the particulars of a seasonally varying heat capacity, once the annual mean
312 value is specified.¹

313 To isolate the factors that can affect the seasonal temperature cycle, we partition the
314 net flux as $F(t, T(t)) = Q(t) - \beta T$ where $Q(t)$ is the seasonal surface flux that is not
315 linearly related to temperature (such as solar radiation) and β is a constant. Physically,
316 $-\beta T$ represents longwave flux, turbulent heat fluxes, and heat transports that damp the
317 temperature response to the seasonal flux cycle. The term crudely represents the temperature
318 dependence of the surface flux and heat transports.

319 After Fourier transforming, we find the following relation for the annual harmonic ($\omega =$
320 $2\pi/(1 \text{ year})$) of T and Q :

$$\begin{aligned} i\omega CT &= Q - \beta T \\ T(\beta + i\omega C) &= Q, \end{aligned} \quad (2)$$

321 which yields the following phase and amplitude relations between T and Q :

¹This was verified by numerically solving the temperature equation with a sinusoidally varying $C(t)$ with different phases.

$$\begin{aligned}\phi_T - \phi_Q &= \arctan \frac{\omega C}{\beta} \\ |T| &= \frac{|Q|}{\sqrt{\beta^2 + \omega^2 C^2}}.\end{aligned}\tag{3}$$

322 The temperature phase lag is set by the ratio of C to β . In the limiting case of small heat
 323 capacity, for which $\omega C/\beta \rightarrow 0$, the temperature is in phase with Q , while for very large heat
 324 capacity, $\omega C/\beta \rightarrow \infty$, and the temperature is in quadrature with Q . The relative amplitude
 325 of temperature to seasonal flux is inversely related to both C and β . To understand the
 326 effects of changes in C and β to the temperature seasonality we linearize and decompose the
 327 variations to Equation 3 to find their dependences on variations in C and β . The result is:

$$\begin{aligned}\Delta\phi_T - \Delta\phi_Q &= \frac{\omega C/\beta}{1 + (\omega C/\beta)^2} \left(\frac{\Delta C}{C} - \frac{\Delta\beta}{\beta} \right) \\ \frac{\Delta|T|}{|T|} - \frac{\Delta|Q|}{|Q|} &= \frac{-1}{1 + (\omega C/\beta)^2} \left(\left(\frac{\omega C}{\beta} \right)^2 \frac{\Delta C}{C} + \frac{\Delta\beta}{\beta} \right).\end{aligned}\tag{4}$$

328 Assuming small variations in β and ϕ_Q , an increase in heat capacity will cause a phase
 329 delay. Likewise, for small variations in β and $|Q|$, an increase in C will lead to a decreased
 330 amplitude. Thus we see that heat capacity changes have opposite effects on phase and
 331 amplitude and that if phase and amplitude do not change in opposite ways, this implies
 332 that effective heat capacity changes are not the dominant effect. We can quantify this: since
 333 $\omega C/\beta$ is around 0.5 in the models, variations in C are dominant when $\Delta C/C \gg 4\Delta\beta/\beta$.

334 We have seen in the previous section that at high latitudes the temperature cycle is
 335 slowed and damped (more over ocean than land), which is qualitatively consistent with an
 336 increase in effective heat capacity. These seasonality changes occur in the same regions in
 337 which sea ice decreases in extent, thins, or becomes less persistent throughout the year. We
 338 will show below in more quantitative, greater detail that an effective heat capacity increase
 339 due to sea ice loss is most likely driving the phase delay and weakened amplitude of the
 340 temperature cycle at high latitudes and in the global mean.

341 The temperature cycle changes are different in the tropics and subtropics. We have
342 already made the case that since phase and amplitude both increase in these regions, these
343 temperature cycle changes must be forced at least in part by something other than changes
344 in effective heat capacity. We provide evidence that this may be a consequence of a fractional
345 increase in β that is nearly an order of magnitude larger than the local fractional reduction
346 in effective heat capacity.

347 The dividing line between these two regions meanders longitudinally, but is approximately
348 between 45° – 60° . While sea ice extent varies with time, longitude, and hemisphere, the extent
349 of late 20th century sea ice is approximately around 60° , marking the top of the transition
350 zone. Below we focus on the high and low latitudes separately due to the different nature of
351 their temperature annual cycle changes.

352 *a. High latitudes*

353 Before demonstrating that the high-latitude phase delay and amplitude decrease are due
354 to sea ice loss we demonstrate that they are not directly due to changes in the surface flux
355 cycle. For the flux to be responsible for the high-latitude seasonality changes to temperature,
356 seasonal surface flux would need to delay and weaken. In fact, the reverse happens, as shown
357 in Figure 8(a) and (b).

358 There is little change in the phase of surface flux at high latitudes. In fact, the phase is
359 actually advancing over some high-latitude ocean regions, indicating that the high-latitude
360 temperature phase delay is not being driven by changes in the surface flux phase. The surface
361 flux amplitude, on the other hand, does show robust changes in the high latitudes. These
362 changes, however, are of the opposite sign to the temperature amplitude changes. Over
363 high-latitude ocean in both hemispheres, the surface flux amplitude increases by around
364 50% in both hemispheres. The increase is confined to ocean and is in the same region as the
365 reduction in the amplitude of surface temperature. Since the phase and amplitude changes of
366 surface flux are of the opposite sign to the temperature changes, they cannot be responsible

367 for the latter.

368 In terms of our energy balance model, Figure 8(a) and (b) show the seasonality changes to
369 $F = Q - \beta T$. The seasonality changes to $Q(t)$ are similar to $F(t)$ at high latitudes. Whether
370 we take $Q(t)$ to be the net shortwave flux at the surface or at the top of the atmosphere, we
371 find the same small phase advance and large amplitude increase in the high latitudes (not
372 shown). In Equation 4, this means that $\Delta\phi_Q$ is a small negative number and that $\Delta|Q|/|Q|$
373 is a large positive number. Hence we can rule out seasonal changes of Q as responsible for
374 driving the high-latitude seasonal temperature changes.

375 The surface flux amplitude changes at high latitudes in Figure 8(b) are consistent with
376 sea ice loss (Screen and Simmonds 2010). Climatologically, the ice margin is not only the
377 region of greatest upward turbulent heat flux during the winter, but also where the total
378 surface flux amplitude is greatest. As the ice edge shifts poleward during the 21st century,
379 the consequence to the surface flux is an increase in amplitude in the polar ocean and a
380 decrease in amplitude in the sub-polar ocean (Deser et al. 2010). In the polar ocean, the
381 albedo is also reduced, which increases the downward shortwave radiation at the surface
382 during the summer, contributing to an increased surface flux amplitude at high latitudes.

383 In the multi-model mean, the surface temperature has a phase delay and amplitude
384 decrease at high latitudes, consistent with an effective heat capacity increase. We also
385 look for this consistency on an individual model basis. For example, do models with large
386 phase delays also tend to have large amplitude decreases? We address this question in
387 Figure 9. On the y-axis we plot $\Delta\phi = \Delta\phi_T - \Delta\phi_Q$, the change in the phase of the surface
388 temperature relative to the change in phase of seasonal surface flux and on the x-axis we plot
389 $\Delta A = \Delta(|T|/|Q|)$, the change in the ratio of amplitudes of surface temperature to seasonal
390 surface flux. The phase and amplitude changes are averaged over the NH and SH oceanic
391 polar caps for each model. We find correlations between the phase and amplitude changes
392 for both polar caps: $r = -0.67$ in the NH and $r = -0.79$ in the SH. Results are similar if
393 we plot $\Delta\phi_T$ against $\Delta|T|$, though the correlations rise to $r = -0.79$ in the NH and fall to

394 $r = 0.17$ in the SH. There is only one model where $\Delta\phi$ and ΔA have the same sign, and
 395 both phase and amplitude changes in that model are small.

396 If the ϕ and A changes were entirely due to an effective heat capacity change we would
 397 expect the changes to be linearly related with slope $-\beta\sqrt{1 + (\beta/\omega C)^2}$, represented by the
 398 dotted line in Figure 9; we use the multi-model mean of the above quantity to compute the
 399 theoretical slope. The theoretical slope (-0.08) is much flatter than the slope of the best
 400 fit line (-0.40) in the NH, while for the SH the slopes are more similar (-0.16 theoretically
 401 and -0.26 for the best-fit line). We do not completely understand why the theoretical and
 402 best-fit slopes differ so much in the NH. An obvious possibility is that our very simple,
 403 zero-dimensional, two-parameter model is inadequate to capture the GCM behavior at this
 404 quantitative level; another is that the multi-model mean is not the most appropriate estimate
 405 of β to use to compute the theoretical slope. Nonetheless, that the changes in phase and
 406 amplitude are negatively correlated qualitatively supports the hypothesis that heat capacity
 407 changes control the seasonality changes. A change in β alone would produce a positive
 408 correlation, and surface flux amplitude changes alone would not be expected to change the
 409 phase to the extent that the response is linear.

410 To further understand whether seasonality changes are due to C or β , we calculate the
 411 changes to effective heat capacity in the context of our energy balance model. Solving
 412 Equation 3 for C and β in terms of phase and amplitude gives the following.

$$\begin{aligned}
 C &= \frac{\sin \phi}{\omega A} \\
 \beta &= \frac{\cos \phi}{A}
 \end{aligned}
 \tag{5}$$

413 Since we calculate A and ϕ directly via Fourier transform, Equation 5 gives expressions
 414 for the C and β changes for the CMIP3 models in the context of this simple temperature
 415 model.

416 In our calculations we take Q to be the net shortwave flux at the surface, but the results
 417 are nearly the same if we take it to be the net shortwave flux at the top of the atmosphere.

418 For both the surface temperature and the net surface shortwave flux we calculate the average
419 phase and amplitude over ocean poleward of 60° for each hemisphere for the last two decades
420 of the 20th and 21st centuries. From these values we find C and β and plot the changes in
421 Figure 10(a).

422 As in previous plots for the high latitudes, there is a robust phase delay and amplitude
423 reduction among the models. Changes to C show a robust increase among the models in
424 both hemispheres; nearly every single model predicts an increase in effective heat capacity.
425 The multi-model mean increases are 82% and 43% for the NH and SH, respectively. Changes
426 to β are smaller, but no less robust. The multi-model mean increase is 16% for the NH and
427 9% for the SH. We interpret the β changes mathematically as an increased damping in the
428 system, and physically as the turbulent and longwave fluxes and heat transports - in some
429 combination - becoming more effective at returning the surface temperature to equilibrium.
430 Which of the processes involved is most responsible for this change, and how the change is
431 ultimately forced by greenhouse gas increases is not yet clear and will require further study.

432 Despite the robust increase in β , the proportionally larger increase in C has the greater in-
433 fluence on the changes in the seasonality of temperature at high latitudes. From Equation 4,
434 phase delays are proportional to $\Delta C/C - \Delta\beta/\beta$, indicating that if β did not change, the phase
435 delay would be even larger. Amplitude changes are proportional to $-\Delta\beta/\beta - (\omega C/\beta)^2 \Delta C/C$,
436 where $(\omega C/\beta)^2$ is a proportionality factor averaging 0.4 for the NH and 0.7 for the SH
437 in the 20th century. Since β and C both increase in the 21st century, both are respon-
438 sible for a decreased amplitude. However, when we calculate the multi-model mean of
439 $(\omega C/\beta)^2 (\Delta C/C) (\Delta\beta/\beta)^{-1}$ we find that the contribution from the heat capacity change
440 term is two to three times larger than that from the β term.

441 Sea ice loss was postulated to be the reason for high latitude changes in seasonality by
442 earlier authors (Manabe and Stouffer 1980; Manabe et al. 1992; Mann and Park 1996). The
443 explanation goes as follows: sea ice acts as a partition between the atmosphere and ocean
444 by shutting off radiative transfer and turbulent heat fluxes between the two domains. The

445 only coupling is by conduction through the sea ice. As sea ice melts, the insulating effect
446 wanes and the ocean and atmosphere can more freely exchange heat, raising the effective
447 heat capacity of the surface. Any external addition of heat, such as from solar radiation,
448 will more easily be shared between the atmosphere and ocean if there is less sea ice. Sea ice
449 loss is robust in the models: sea ice area diminishes in every model at a roughly linear rate
450 during the 21st century (Figure 11). The NH suffers a larger ice loss than the SH, which
451 may partly account for why the amplitude and phase changes are larger in the NH.

452 If all of the effective heat capacity increase were due to sea ice loss, then $\Delta C/C$ would
453 be roughly proportional to the fractional change in open ocean area. We calculate the latter
454 quantity for each model and in Figure 12 plot it against the fractional change in effective
455 heat capacity for each model as calculated from Equation 5.

456 The two calculations of effective heat capacity correlate well with each other, indicating
457 that sea ice loss is probably the dominant mechanism for the effective heat capacity change.
458 While the correlations are strong, the models do exhibit a bias: the two effective heat capacity
459 calculations aren't randomly distributed about the one-to-one line, but instead the effective
460 heat capacity change is larger when calculated from Equation 5. This could be due to the
461 limitations of relating effective heat capacity increase to ice area alone. For example, simply
462 measuring the open ocean increase does not take into account sea ice thinning, which would
463 increase the effective heat capacity relative to a thick sea ice layer. Regardless, sea ice area
464 loss appears to account for most of the effective heat capacity increase which is driving the
465 delayed and weakened annual temperature cycle in the high latitudes.

466 Another way to quantify the relationship between temperature annual cycle changes and
467 sea ice changes is to correlate the two across models in the ensemble. We focus on high-
468 latitude (poleward of 60°) annual cycle changes to air temperature over ocean in order to
469 determine if models with large sea ice loss tend to have large phase delays and weak annual
470 cycles. We find that correlations of temperature phase delay with annual sea ice area change
471 are significant for the NH ($r = -0.67$), but not for the SH ($r = -0.35$) at the 95% level

472 (Figure 13(a)). Correlations between amplitude change and sea ice area change are $r = 0.51$
473 for the NH and $r = 0.46$ for the SH and are significant for both hemispheres (Figure 13(b)).
474 The correlations do not significantly change if we weight the area loss with a factor to account
475 for the reduction of ice thickness.

476 *b. Low Latitudes*

477 While sea ice loss seems to explain the high-latitude phase and amplitude changes of the
478 annual temperature cycle, it does not directly explain the changes at low latitudes. Equa-
479 torward of roughly 45° the models expect a slight phase delay and an increased amplitude.
480 One possible explanation for this behavior is that the high-latitude seasonality changes are
481 transported equatorward, for example, by midlatitude eddies. There are two reasons this
482 is unlikely. For one, the amplitude increases at low latitudes, while it decreases near the
483 poles. The other reason is that models that have large delays in the high latitudes do not
484 tend to have large delays in the subtropics. The only region-to-region phase correlations
485 that appear significant are between the extratropics and subtropics in the Northern Hemi-
486 sphere ($r = 0.59$). But the amplitude correlations are small between these two regions
487 ($r = 0.17$), suggesting that the delay in the low latitudes is not simply communicated from
488 higher latitudes.

489 An alternate explanation is that the temperature seasonality changes are a result of
490 surface flux seasonality changes. While the phase and amplitude of surface flux changes
491 are opposite in sign to those of the temperature changes at high latitudes, this is not the
492 case at low latitudes as shown in Figure 8. Both the phase of surface temperature and
493 surface flux show a small delay of less than 5 days from 45°S – 45°N . The amplitude changes
494 of temperature and surface flux are even more similar. From 45°S – 45°N both temperature
495 and surface flux amplitude show broad increases of around 5%.

496 There is also a strong spatial correlation between the temperature and flux changes. Ro-
497 bust phase delays occur in the same places such as the Eastern Pacific and the NH subtropical

498 Atlantic. The temperature and flux also both have especially large amplitude increases in the
 499 Eastern Pacific and Eastern Atlantic. We create a measure of spatial correlation in Figure 14
 500 by plotting the multi-model mean seasonality changes for temperature and flux against one
 501 another for all subtropical ocean grid boxes between 15° – 30° in both hemispheres, not in-
 502 cluding locations where the annual cycle is small. There are strong correlations of $r = 0.67$
 503 for the phases and $r = 0.78$ for the amplitudes, indicating that the surface flux changes are
 504 spatially correlated with the surface temperature changes.

505 We can understand these changes in the context of our energy balance model. While
 506 the seasonal cycle of total flux, F , delays and strengthens in the subtropics in Figure 8, the
 507 same cannot be said of the temperature-independent component of the flux, Q . There is
 508 almost no change in the phase or amplitude of the net shortwave radiation at the surface
 509 (not shown). Since $F = Q - \beta T$, this suggests that changes in β are responsible for the
 510 changes in total surface flux.

511 To find the explicit changes to C and β , we use the same procedure as for the high
 512 latitudes by calculating C and β from A and ϕ with Equation 5 and plot these results in
 513 Figure 10(b). The phase delay is around 2.8 days in the NH and 1.6 days in the SH, while the
 514 amplitude increase is around 3–4% for both the NH and SH. While small, these changes are
 515 robust in the models: the vast majority have the same sign as the mean change. Unlike in
 516 the high latitudes, we find a small decrease in the subtropical heat capacity around 2–3% in
 517 both hemispheres. This might be a consequence of a reduction in tropical ocean mixed layer
 518 depth (Philip and Oldenborgh 2006). The larger changes are in β , which decreases by 20%
 519 in the NH and 12% in the SH. Since $\Delta\phi \propto \Delta C/C - \Delta\beta/\beta$, we can attribute the subtropical
 520 phase delay primarily to the β decrease. Likewise, since $\Delta A/A \propto -\Delta\beta/\beta - (\omega C/\beta)^2 \Delta C/C$,
 521 and $\omega C/\beta < 1$, the amplitude increase is also primarily due to the β decrease.

522 The reduction in β indicates that 21st century temperature in the subtropics becomes
 523 more weakly damped. Physically, a weakened β means that the combination of turbulent and
 524 latent fluxes and heat transports become less effective at returning the surface temperature

525 to equilibrium. A reduced β does not necessarily imply a weakened surface flux amplitude
526 because the total surface flux $F = Q - \beta T$ also depends on the phase relationship between T
527 and Q . For the low latitudes, the surface flux amplitude increases despite the reduction in β .
528 Sobel and Camargo (2011) presented evidence that the surface flux amplitude increases are
529 driven by changes in the seasonal cycle of surface winds, with subtropical winds increasing
530 in the winter hemisphere and decreasing in the summer hemisphere. At a fixed subtropical
531 location, these changes in wind speed change sign over the year and thus will not be described
532 well by a simple change in an otherwise constant coefficient β . Further, because surface air
533 humidity (the other state variable that enters bulk formulae for the surface latent heat flux,
534 besides wind speed and SST) can adjust so quickly to other factors, it may be appropriate
535 to view these wind speed changes as an external forcing on the surface fluxes, rather than a
536 change in a damping coefficient in an SST equation. These considerations suggest that the
537 simple model we have proposed to interpret the high-latitude seasonality changes projected
538 by the models may be inadequate to capture the low-latitude changes. Further work is
539 required to determine the exact roles of the surface wind and other factors in the surface
540 energy budget. It is clear, however, that there is a link between the net surface heat flux and
541 the seasonal temperature cycle at low latitudes, unlike at high latitudes where the effective
542 heat capacity governs the changes in seasonality.

543 **6. Conclusion**

544 In this study we analyzed the changes to the seasonality of surface temperature in re-
545 sponse to an increase in greenhouse gases during the 21st century as represented by CMIP3
546 models. We found large, robust, global changes to the annual cycle of surface temperature:
547 a phase delay and an amplitude reduction. By analyzing these changes geographically, we
548 found that the phase delay and amplitude decrease are strongest at high latitudes and drive
549 the global response. These polar changes are consistent with an effective heat capacity in-

550 crease of the surface layer due to sea ice loss. At low latitudes there is a small phase delay
551 and an amplitude increase, which we linked to changes in the seasonality of the surface heat
552 flux.

553 CMIP3 climate models accurately represent the typical phase and amplitude of the an-
554 nual cycle aloft and at the surface as represented by the ERA-40 reanalysis. Geographic
555 variations in models and observations are spatially consistent and can be traced to different
556 surface effective heat capacities: temperature over ocean responds slowly and weakly, while
557 temperature over land and sea ice responds rapidly and strongly.

558 At high latitudes the temperature cycle delays and weakens in response to greenhouse
559 gases in the CMIP3 models. We provided evidence that sea ice loss is driving these changes.
560 By fitting CMIP3 data to a parameterized surface energy balance model, we found that
561 an increase in effective heat capacity primarily accounts for the phase delay and amplitude
562 increase at high latitudes. We also demonstrated that the increase in effective heat capacity
563 for each model was consistent with the increase in open-ocean fraction, indicating that sea
564 ice loss is driving the effective heat capacity and seasonality changes at high latitudes. We
565 provided further evidence of this mechanism by showing strong correlations between sea
566 ice loss and phase and amplitude changes among the models at the high latitudes in each
567 hemisphere.

568 The projected delayed and weakened temperature cycle in the high-latitudinal NH is a
569 manifestation of Arctic Amplification, the accelerated annual mean warming in the Arctic
570 Ocean relative to the rest of the globe robustly predicted by 21st century climate simulations.
571 Arctic Amplification has a seasonal component to it as well, with models predicting little
572 warming in summer and substantial warming during the late fall and early winter (Serreze
573 and Francis 2006). This warming structure is consistent with the changes in the annual
574 harmonic of phase and amplitude. While the models predict the surface annual cycle changes
575 to grow over the course of the 21st century, recent studies have already found early signs
576 of changes in the Arctic Ocean. Among four different data sets, Serreze et al. (2009) and

577 Screen and Simmonds (2010) found evidence of a delayed and weakened temperature cycle
578 in the Arctic Ocean, consistent with rapid sea ice loss over this time period and providing
579 support for future changes expected by the CMIP3 models.

580 We suggest that the high-latitude seasonal temperature changes are credible. Not only are
581 they robust among the models, but they are also linked to a robust response in the models:
582 sea ice loss. While there has been some disagreement between models and observations of
583 temperature phase changes over midlatitude NH land during the 20th century (Stine et al.
584 2009), substantial sea ice loss is already occurring in the Arctic. Furthermore, trends of an
585 Arctic temperature phase delay and amplitude decrease have been observed during the last
586 30 years.

587 Changes in the temperature cycle at low latitudes are different in nature than those at
588 high latitudes. While still robust, they have a small phase delay and a small amplitude
589 increase. Because the changes in phase and amplitude are both positive, they are not consis-
590 tent with an increase in effective heat capacity. However, they are consistent with a delayed
591 and strengthened surface flux cycle that we traced to a decrease in damping of surface tem-
592 perature by turbulent and longwave heat fluxes in our energy balance model. We also found
593 a strong spatial correlation between seasonality changes in surface flux and surface temper-
594 ature in the subtropics. Sobel and Camargo (2011) describe a link between changes in the
595 amplitude of the seasonal cycle in SST and those in surface wind speed and describe the
596 latter as a consequence of the expansion of the Hadley cell. While we do not understand
597 the mechanism responsible for the phase changes in the net surface flux, it is worth further
598 effort to do so. Projected phase delays of surface temperature in the tropics appear to be
599 associated with similar phase delays in the onset and demise dates of monsoons (Biasutti
600 and Sobel 2009).

601 *Acknowledgments.*

602 This research was supported by NSF Grant AGS-0946849 and NASA Earth and Space

603 Science Fellowship NNX11AL88H. We acknowledge the modeling groups, the Program for
604 Climate Model Diagnosis and Intercomparison (PCMDI) and the WCRP's Working Group
605 on Coupled Modelling (WGCM) for their roles in making available the WCRP CMIP3 multi-
606 model dataset. Support of this dataset is provided by the Office of Science, U.S. Department
607 of Energy. The ERA-40 data was provided by ECMWF.

REFERENCES

- 610 Biasutti, M. and A. Sobel, 2009: Delayed Sahel rainfall and global seasonal cycle in a warmer
611 climate. *Geophys. Res. Lett.*, **36**, L23707, doi:10.1029/2009GL041303.
- 612 Carson, J. and H. Moses, 1963: The annual and diurnal heat-exchange cycles in upper
613 layers of soil. *J. Appl. Meteor.*, **2 (3)**, 397–406, doi:10.1175/1520-0450(1963)002(0397:
614 TAADHE)2.0.CO;2.
- 615 Chiang, J., Y. Kushnir, and A. Giannini, 2002: Deconstructing Atlantic Intertropical Con-
616 vergence Zone variability: Influence of the local cross-equatorial sea surface tempera-
617 ture gradient and remote forcing from the eastern equatorial Pacific. *J. Geophys. Res.*,
618 **107 (D1)**, 4004, doi:10.1029/2000JD000307.
- 619 Deser, C., R. Tomas, M. Alexander, and D. Lawrence, 2010: The seasonal atmospheric
620 response to projected Arctic sea ice loss in the late twenty-first century. *J. Climate*, **23 (2)**,
621 333–351, doi:10.1175/2009JCLI3053.1.
- 622 Donohoe, A. and D. S. Battisti, 2012: The seasonal heating of the atmosphere. *J. Climate*,
623 in preparation.
- 624 Eicken, H., 2008: From the microscopic, to the macroscopic, to the regional scale: Growth,
625 microstructure and properties of sea ice. *Sea Ice*, D. N. Thomas and G. S. Dieckmann,
626 Eds., Blackwell Science Ltd, 22–81, doi:10.1002/9780470757161.ch2.
- 627 Fitter, A. H. and R. S. R. Fitter, 2002: Rapid changes in flowering time in British plants.
628 *Science*, **296 (5573)**, 1689–1691, doi:10.1126/science.1071617.
- 629 Kutzbach, J., 1967: Empirical eigenvectors of sea-level pressure, surface temperature and
630 precipitation complexes over North America. *J. Appl. Meteor.*, **6**, 791–802.

- 631 Loon, H. V., 1967: The half-yearly oscillations in middle and high southern latitudes and
632 the coreless winter. *J. Atmos. Sci.*, **24**, 472–486.
- 633 Manabe, S., M. Spelman, and R. Stouffer, 1992: Transient responses of a coupled ocean-
634 atmosphere model to gradual changes of atmospheric CO₂. Part II: Seasonal response. *J.*
635 *Climate*, **5 (2)**, 105–126.
- 636 Manabe, S. and R. Stouffer, 1980: Sensitivity of a global climate model to an increase of
637 CO₂ concentration in the atmosphere. *J. Geophys. Res.*, **85 (C10)**, 5529–5554.
- 638 Mann, M. and J. Park, 1996: Greenhouse warming and changes in the seasonal cycle of
639 temperature: Model versus observations. *Geophys. Res. Lett.*, **23 (10)**, 1111–1114.
- 640 Meehl, G., C. Covey, T. Delworth, M. Latif, B. McAvaney, J. Mitchell, R. Stouffer, and
641 K. Taylor, 2007: The WCRP CMIP3 multimodel dataset. *Bull. Am. Meteorol. Soc.*, **88**,
642 1383–1394.
- 643 Philip, S. and G. V. Oldenborgh, 2006: Shifts in ENSO coupling processes under global
644 warming. *Geophys. Res. Lett.*, **33**, L11704, doi:10.1029/2006GL026196.
- 645 Screen, J. and I. Simmonds, 2010: Increasing fall-winter energy loss from the Arctic Ocean
646 and its role in Arctic temperature amplification. *Geophys. Res. Lett.*, **37**, L16707, doi:
647 10.1029/2010GL044136.
- 648 Serreze, M., A. Barrett, J. Stroeve, D. Kindig, and M. Holland, 2009: The emer-
649 gence of surface-based Arctic amplification. *The Cryosphere*, **3 (1)**, 11–19, doi:10.5194/
650 tc-3-11-2009.
- 651 Serreze, M. and J. Francis, 2006: The Arctic amplification debate. *Clim. Change*, **76 (3)**,
652 241–264, doi:10.1007/s10584-005-9017-y.
- 653 Seth, A., S. Rauscher, M. Rojas, A. Giannini, and S. Camargo, 2011: Enhanced spring

654 convective barrier for monsoons in a warmer world? *Clim. Change*, **104** (2), 403–414,
655 doi:10.1007/s10584-010-9973-8.

656 Sobel, A. and S. Camargo, 2011: Projected future seasonal changes in tropical summer
657 climate. *J. Climate*, **24**, 473–487, doi:10.1175/2010JCLI3748.1.

658 Stewart, I., D. Cayan, and M. Dettinger, 2005: Changes toward earlier streamflow timing
659 across western North America. *J. Climate*, **18** (8), 1136–1155, doi:10.1175/JCLI3321.1.

660 Stine, A. R. and P. Huybers, 2012: Changes in the seasonal cycle of temperature and
661 atmospheric circulation. *J. Climate*, under review.

662 Stine, A. R., P. Huybers, and I. Y. Fung, 2009: Changes in the phase of the annual cycle of
663 surface temperature. *Nature*, **457** (7228), 435–440, doi:10.1038/nature07675.

664 Stroeve, J., M. Holland, W. Meier, T. Scambos, and M. Serreze, 2007: Arctic sea ice decline:
665 Faster than forecast. *Geophys. Res. Lett.*, **34** (9), L09501, doi:10.1029/2007GL029703.

666 Thomson, D., 1995: The seasons, global temperature, and precession. *Science*, **268** (5207),
667 59.

668 Trenberth, K., 1983: What are the seasons?. *Bull. Am. Meteor. Soc.*, **64**, 1276–1277.

669 Uppala, S., et al., 2005: The ERA-40 re-analysis. *Quart. J. Roy. Meteor. Soc.*, **131** (612),
670 2961–3012, doi:10.1256/qj.04.176.

671 List of Figures

- 672 1 Hemispherically averaged, multi-model mean monthly surface air temperature
673 anomaly over ocean in °C for the last two decades of the 20th (gray) and 21st
674 (black) centuries. Both the NH (solid line) and SH (dashed line) have a phase
675 delay and amplitude decrease. 32
- 676 2 The 1958-2001 mean temperature phase from insolation (in days) for (a) the
677 ERA-40 reanalysis of observations and (b) the CMIP3 multi-model mean,
678 with the difference between the two shown in (c). The mean amplitude (in °C)
679 over the same period for (d) ERA-40, (e) CMIP3, and (f) their difference are
680 plotted in the bottom row. Places where the annual cycle does not represent
681 at least 80% of the total variance are not plotted. 33
- 682 3 Zonal mean surface temperature phase lag from insolation (top, black) and
683 amplitude divided by insolation amplitude (bottom, black). The percent of
684 each latitude band made up of land or sea ice (top and bottom, thick, solid
685 gray) and sea ice alone (top and bottom, thin, dashed gray) are also plotted.
686 The data is for the CMIP3 multi-model mean from 1900-1960, but is repre-
687 sentative of observations as well. Phase and amplitude both correlate strongly
688 with the amount of land and sea ice ($r = -0.90$ and $r = 0.82$, respectively). 34
- 689 4 Climatological mean seasonality, as in Figure 2, except for zonally averaged
690 tropospheric temperature aloft. The top row shows the phase for (a) ERA-40,
691 (b) CMIP3, and (c) their difference. The bottom row shows the amplitude
692 for (d) ERA-40, (e) CMIP3, and (f) their difference. In addition to ignoring
693 locations where the annual cycle is weak, we do not plot the annual cycle in
694 the stratosphere. 35

695	5	Time series of the global surface air temperature (a) lag from insolation and	
696		(b) amplitude calculated with EOFs for all 24 models in the 20C3M and A1B	
697		scenarios. The multi-model mean is in thick black and individual models are	
698		in gray. The solid and dash-dotted lines represent the phase and amplitude	
699		over ocean and land, respectively.	36
700	6	The CMIP3 multi-model mean annual surface temperature (a) phase and (b)	
701		amplitude change between 2080-2099 and 1980-1999. Stippling indicates that	
702		at least 75% of the models share the same sign as the mean change at that	
703		particular location.	37
704	7	As in Figure 6, except for tropospheric seasonality changes for (a) phase and	
705		(b) amplitude.	38
706	8	As in Figure 6, except for total surface flux change, not temperature change.	
707		Only locations where the annual cycle of surface flux represents at least 70%	
708		of the total variance are plotted.	39
709	9	Scatter plot of phase ($\phi_T - \phi_Q$) and amplitude ($ T / Q $) changes for the NH	
710		(black circles) and SH (gray triangles) oceanic polar caps of the CMIP3 models	
711		between the periods 1980–1999 and 2080–2099. Each pair of black and gray	
712		markers represents a single model. The solid lines are the least-squares best	
713		fit line and the dashed lines describe the theoretically predicted slopes as	
714		described in Section 5(a).	40
715	10	Changes in amplitude, phase, effective heat capacity, and β for the NH (black)	
716		and SH (gray) (a) high latitudes and (b) low latitudes over ocean for each	
717		CMIP3 model. The multi-model mean is represented by a bar and individ-	
718		ual models by an “x”. The amplitude and phase are found from a Fourier	
719		transform and the effective heat capacity and β are found from Equation 5.	
720		The changes in phase have been multiplied by 5 to use the same axis for all	
721		quantities. Note that the scale of (a) is 2.5 times that of (b).	41

- 722 11 Time series of annually averaged sea ice area in the (a) NH and (b) SH polar
723 caps (60° – 90°) for the CMIP3 models. The thick black line is the multi-model
724 mean. 42
- 725 12 Scatter plot of fractional effective heat capacity changes in the CMIP3 models
726 calculated from the increase in open ocean fraction on the y-axis and from the
727 amplitude and phase on the x-axis for the NH (black circles) and SH (gray
728 triangles) polar caps. Each marker represents an individual model and the
729 line is the one-to-one line between the axes. Correlations are $r = 0.48$ for the
730 NH and $r = 0.68$ for the SH. The slopes of the lines are 0.55 for the NH and
731 0.32 for the SH. 43
- 732 13 Correlations between sea ice area loss and (a) temperature phase delay and
733 (b) temperature amplitude change for the polar NH (black circles) and polar
734 SH (gray triangles) in the CMIP3 models between 2080–2099 and 1980–1999. 44
- 735 14 Scatter plot of 21st century seasonality changes of surface flux versus surface
736 temperature for (a) phase and (b) amplitude for subtropical ocean grid boxes.
737 There is an area-weighted correlation between these two variables for both
738 phase and amplitude, indicating that, for example, subtropical locations that
739 have large surface flux delays tend to have large surface temperature delays.
740 The data is restricted to 15° – 30° in both hemispheres and does not include lo-
741 cations where the annual harmonic of each variable does not dominate its total
742 variance. The solid line represents the area-weighted least-squares regression. 45

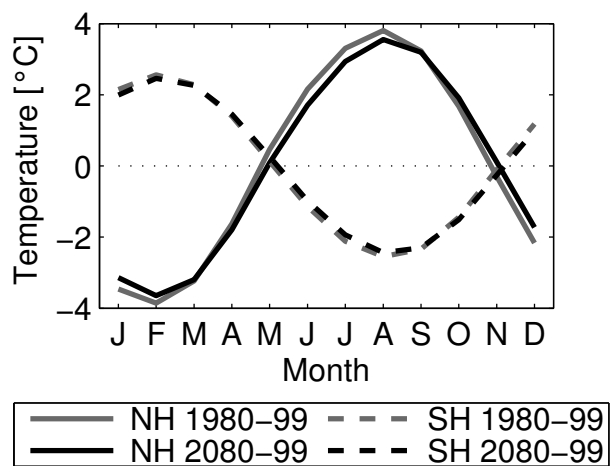


FIG. 1. Hemispherically averaged, multi-model mean monthly surface air temperature anomaly over ocean in °C for the last two decades of the 20th (gray) and 21st (black) centuries. Both the NH (solid line) and SH (dashed line) have a phase delay and amplitude decrease.

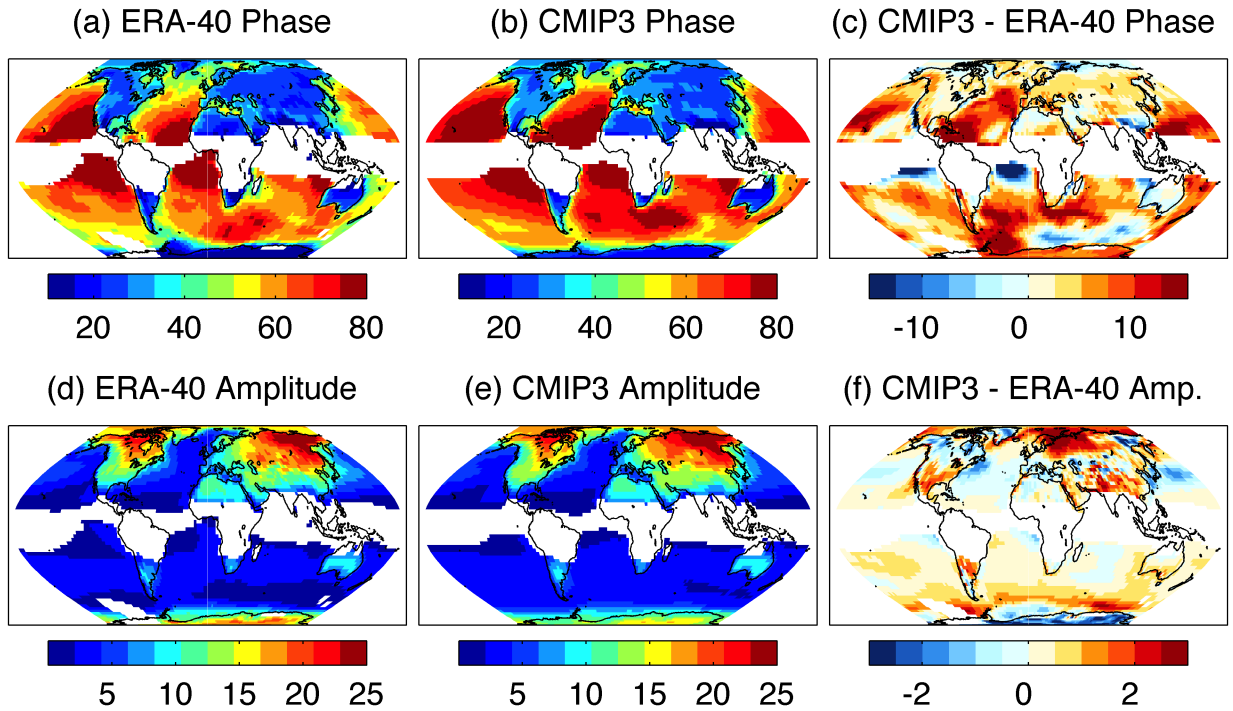


FIG. 2. The 1958-2001 mean temperature phase from insolation (in days) for (a) the ERA-40 reanalysis of observations and (b) the CMIP3 multi-model mean, with the difference between the two shown in (c). The mean amplitude (in °C) over the same period for (d) ERA-40, (e) CMIP3, and (f) their difference are plotted in the bottom row. Places where the annual cycle does not represent at least 80% of the total variance are not plotted.

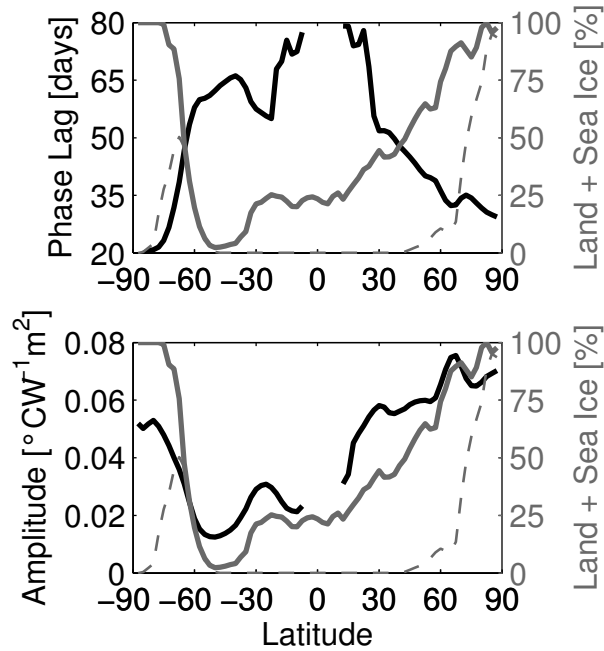


FIG. 3. Zonal mean surface temperature phase lag from insolation (top, black) and amplitude divided by insolation amplitude (bottom, black). The percent of each latitude band made up of land or sea ice (top and bottom, thick, solid gray) and sea ice alone (top and bottom, thin, dashed gray) are also plotted. The data is for the CMIP3 multi-model mean from 1900-1960, but is representative of observations as well. Phase and amplitude both correlate strongly with the amount of land and sea ice ($r = -0.90$ and $r = 0.82$, respectively).

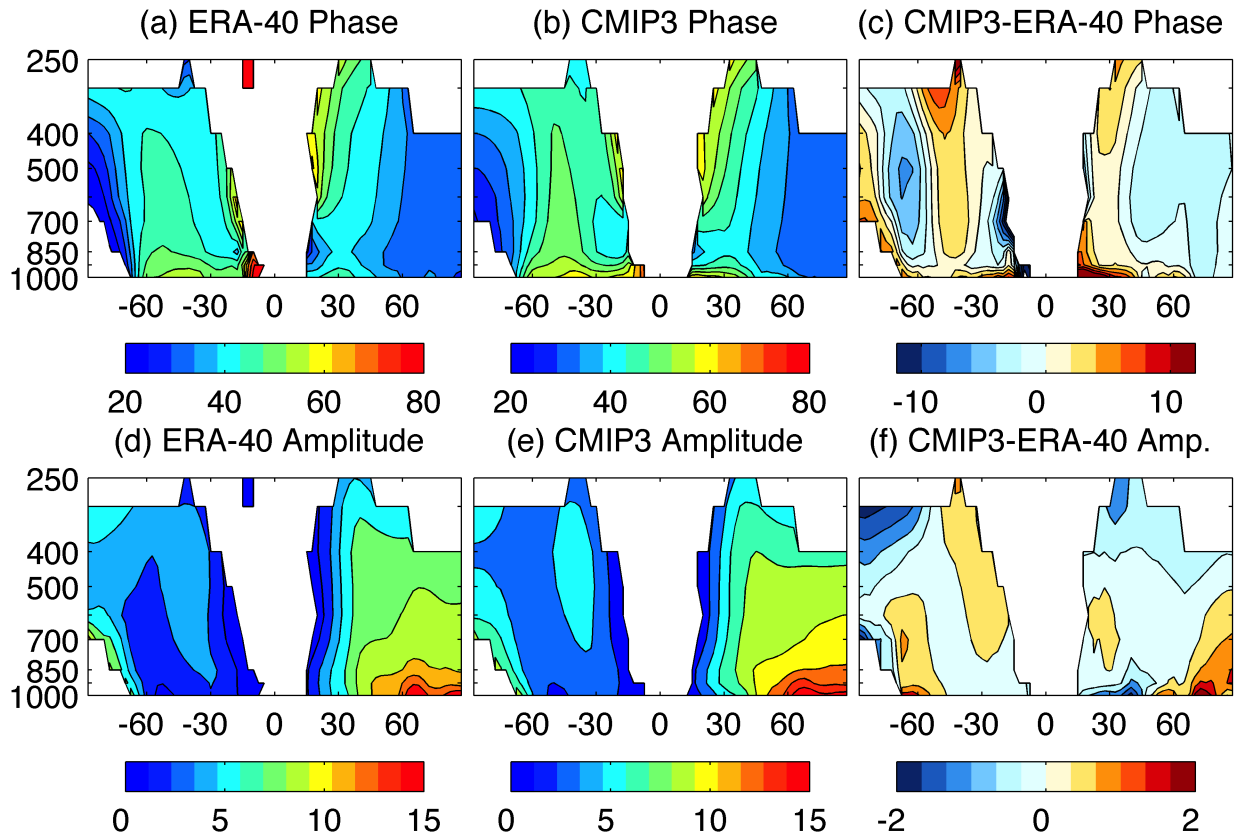


FIG. 4. Climatological mean seasonality, as in Figure 2, except for zonally averaged tropospheric temperature aloft. The top row shows the phase for (a) ERA-40, (b) CMIP3, and (c) their difference. The bottom row shows the amplitude for (d) ERA-40, (e) CMIP3, and (f) their difference. In addition to ignoring locations where the annual cycle is weak, we do not plot the annual cycle in the stratosphere.

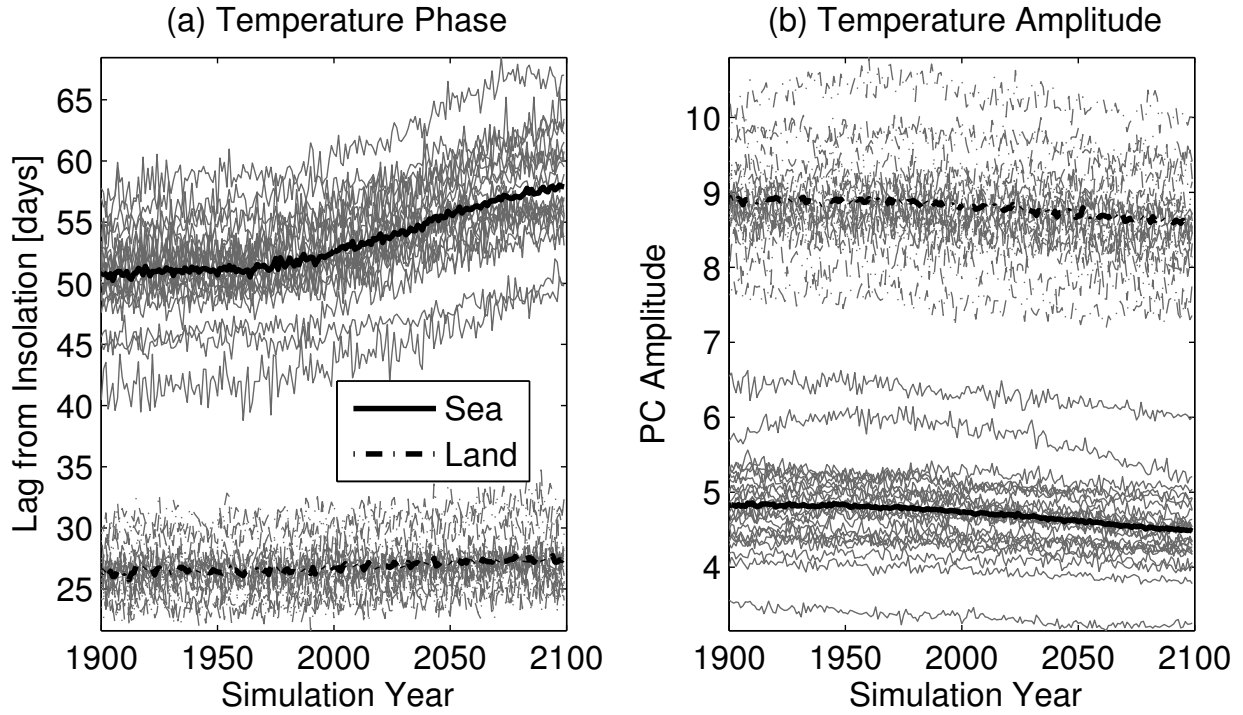


FIG. 5. Time series of the global surface air temperature (a) lag from insolation and (b) amplitude calculated with EOFs for all 24 models in the 20C3M and A1B scenarios. The multi-model mean is in thick black and individual models are in gray. The solid and dash-dotted lines represent the phase and amplitude over ocean and land, respectively.

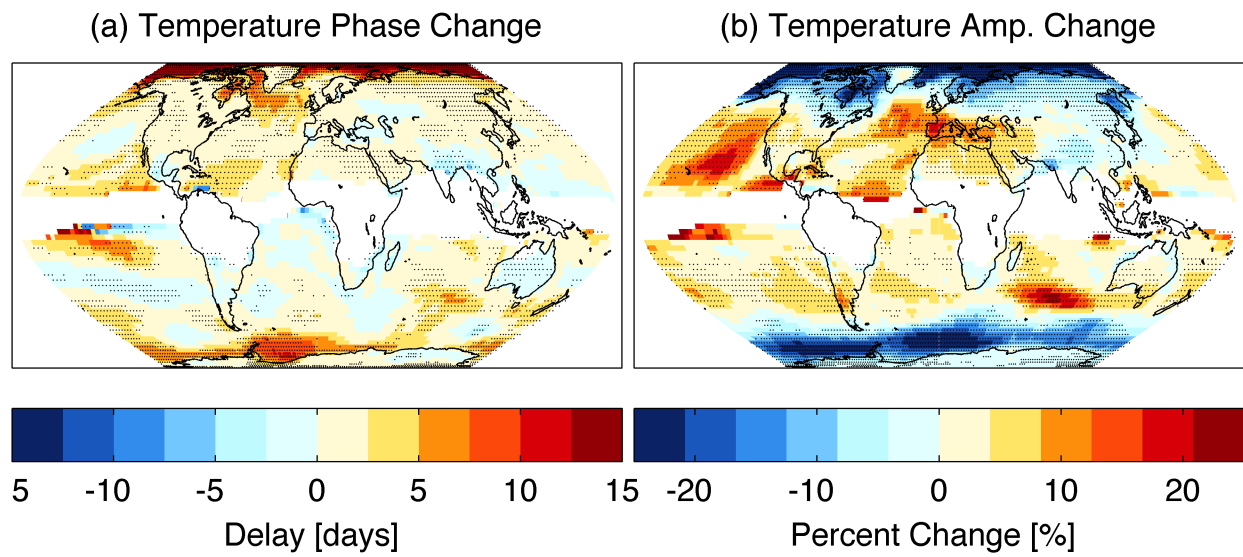


FIG. 6. The CMIP3 multi-model mean annual surface temperature (a) phase and (b) amplitude change between 2080-2099 and 1980-1999. Stippling indicates that at least 75% of the models share the same sign as the mean change at that particular location.

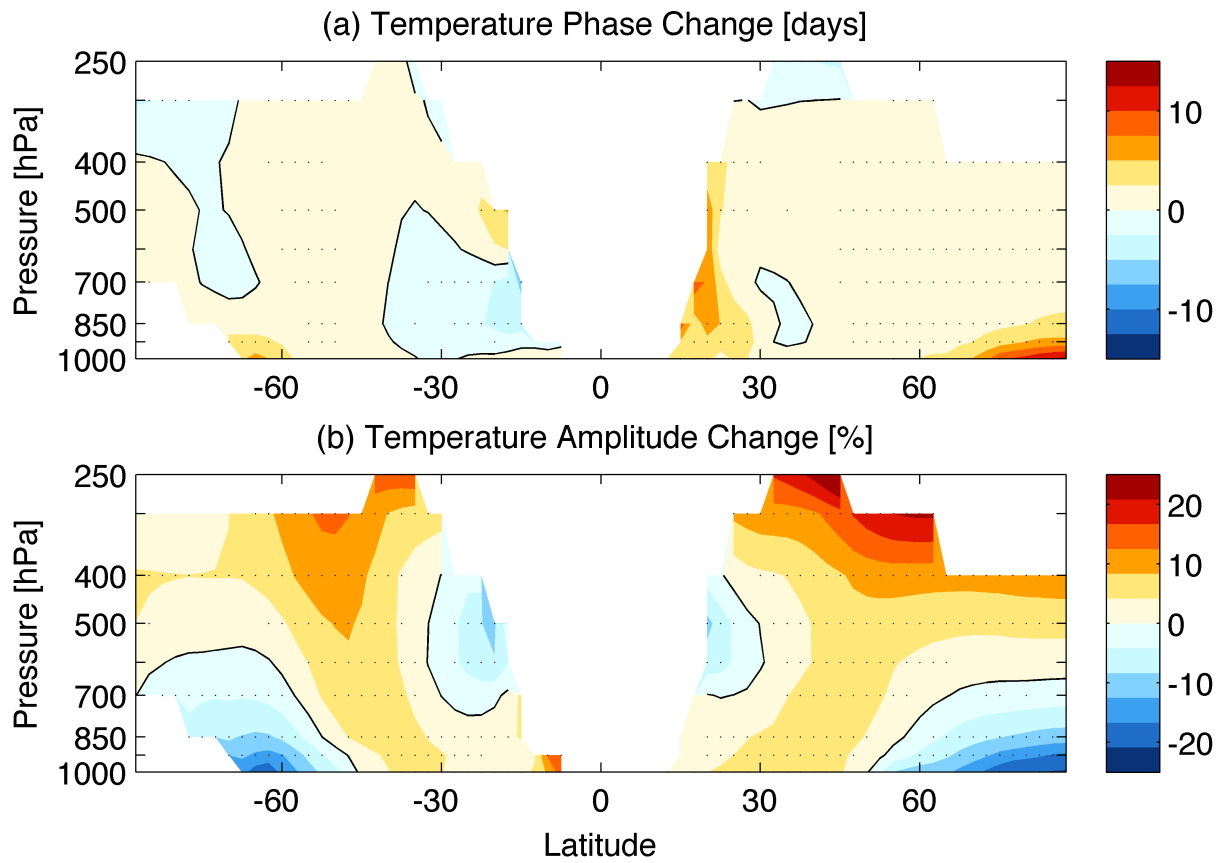


FIG. 7. As in Figure 6, except for tropospheric seasonality changes for (a) phase and (b) amplitude.

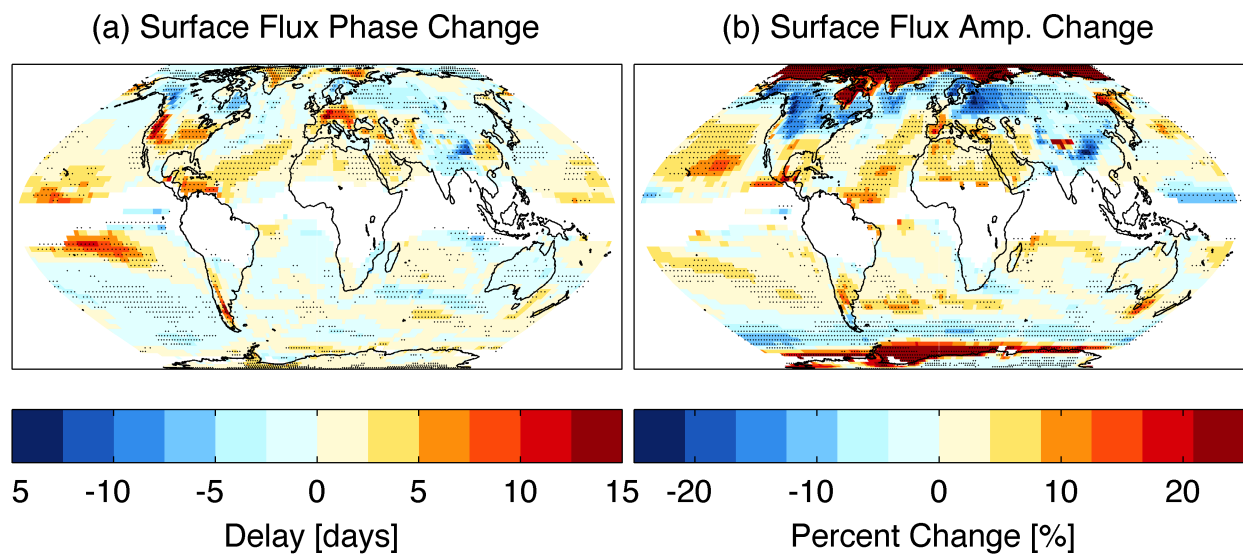


FIG. 8. As in Figure 6, except for total surface flux change, not temperature change. Only locations where the annual cycle of surface flux represents at least 70% of the total variance are plotted.

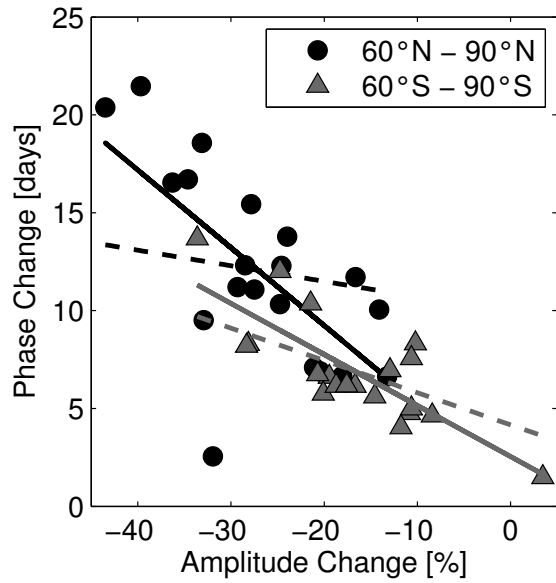


FIG. 9. Scatter plot of phase ($\phi_T - \phi_Q$) and amplitude ($|T|/|Q|$) changes for the NH (black circles) and SH (gray triangles) oceanic polar caps of the CMIP3 models between the periods 1980–1999 and 2080–2099. Each pair of black and gray markers represents a single model. The solid lines are the least-squares best fit line and the dashed lines describe the theoretically predicted slopes as described in Section 5(a).

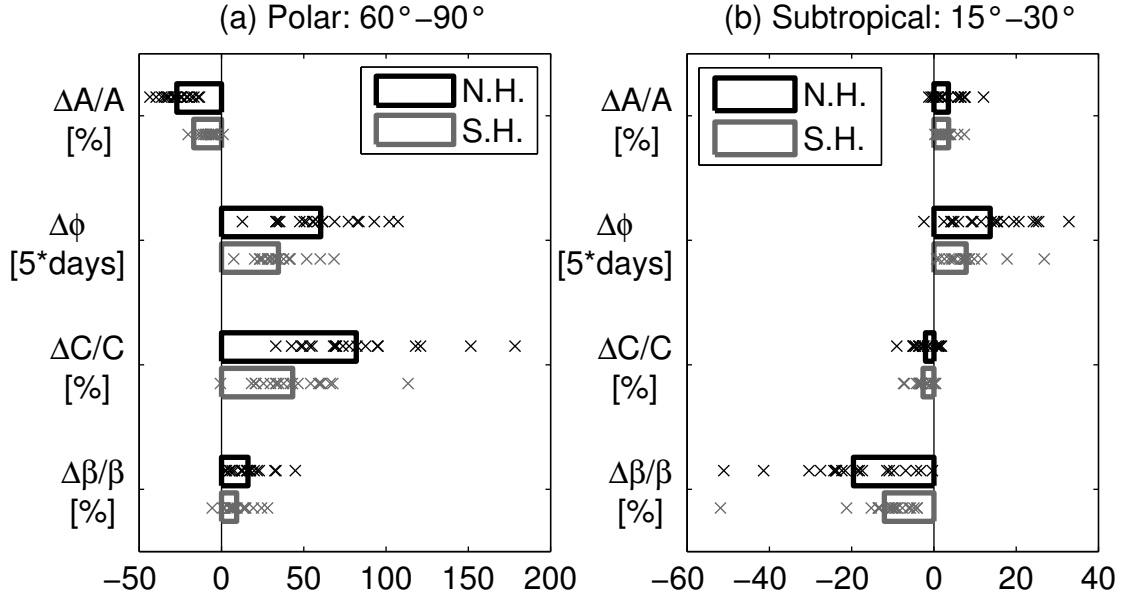


FIG. 10. Changes in amplitude, phase, effective heat capacity, and β for the NH (black) and SH (gray) (a) high latitudes and (b) low latitudes over ocean for each CMIP3 model. The multi-model mean is represented by a bar and individual models by an “x”. The amplitude and phase are found from a Fourier transform and the effective heat capacity and β are found from Equation 5. The changes in phase have been multiplied by 5 to use the same axis for all quantities. Note that the scale of (a) is 2.5 times that of (b).

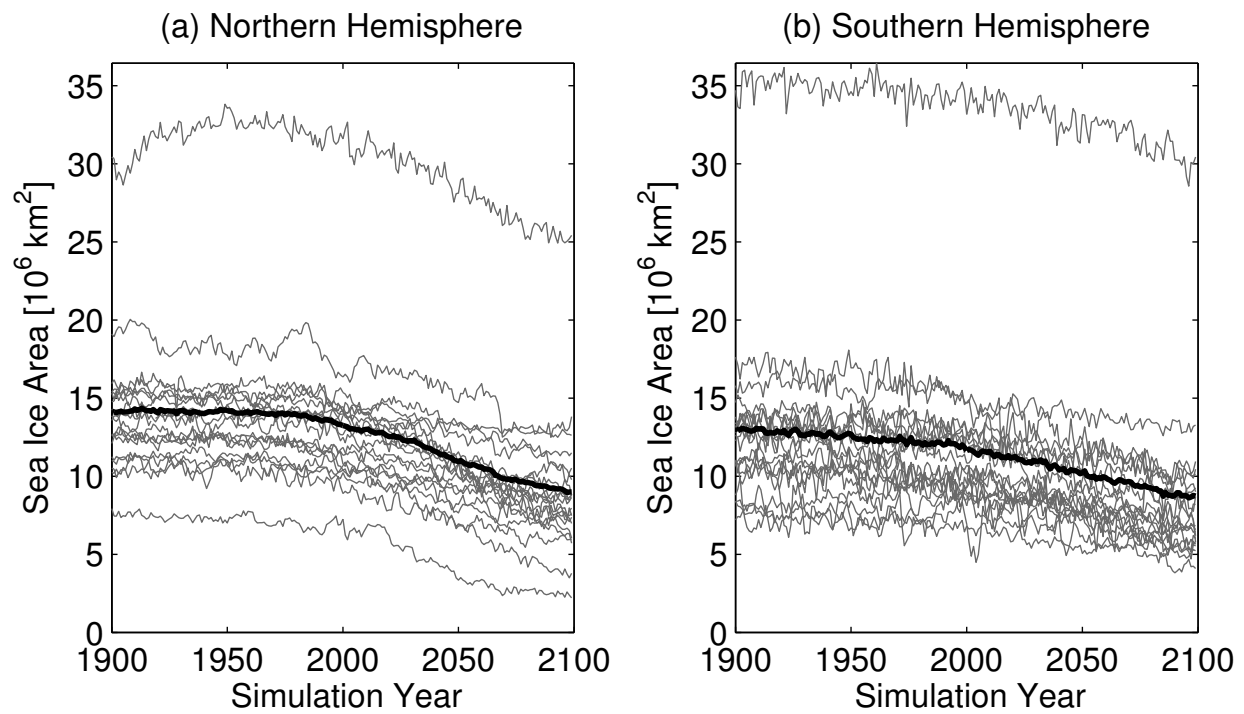


FIG. 11. Time series of annually averaged sea ice area in the (a) NH and (b) SH polar caps (60° – 90°) for the CMIP3 models. The thick black line is the multi-model mean.

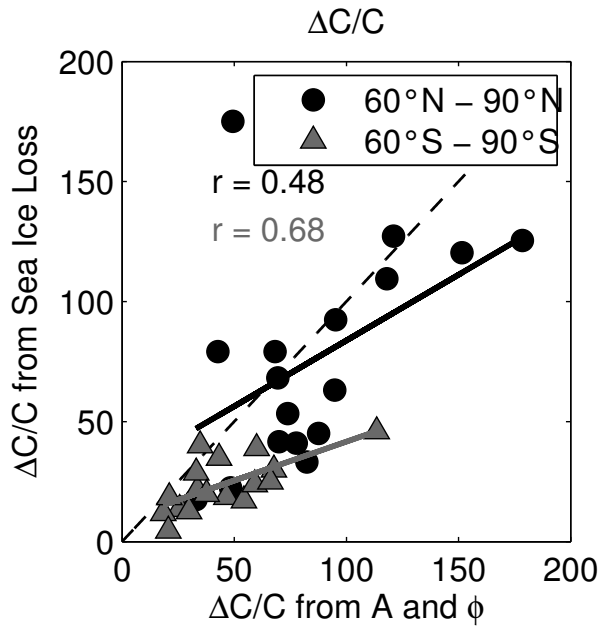


FIG. 12. Scatter plot of fractional effective heat capacity changes in the CMIP3 models calculated from the increase in open ocean fraction on the y-axis and from the amplitude and phase on the x-axis for the NH (black circles) and SH (gray triangles) polar caps. Each marker represents an individual model and the line is the one-to-one line between the axes. Correlations are $r = 0.48$ for the NH and $r = 0.68$ for the SH. The slopes of the lines are 0.55 for the NH and 0.32 for the SH.

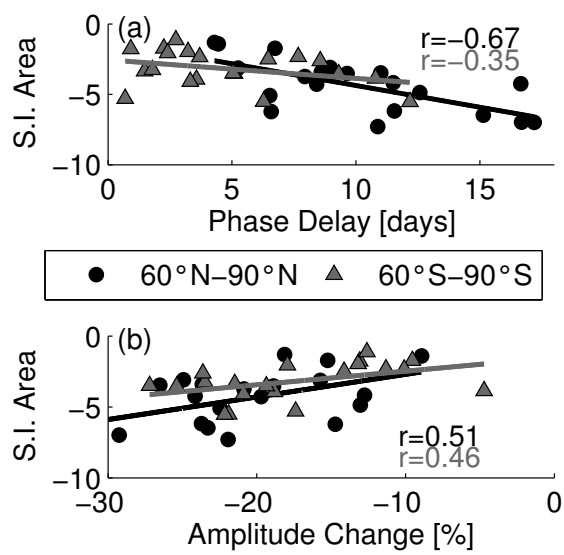


FIG. 13. Correlations between sea ice area loss and (a) temperature phase delay and (b) temperature amplitude change for the polar NH (black circles) and polar SH (gray triangles) in the CMIP3 models between 2080–2099 and 1980–1999.

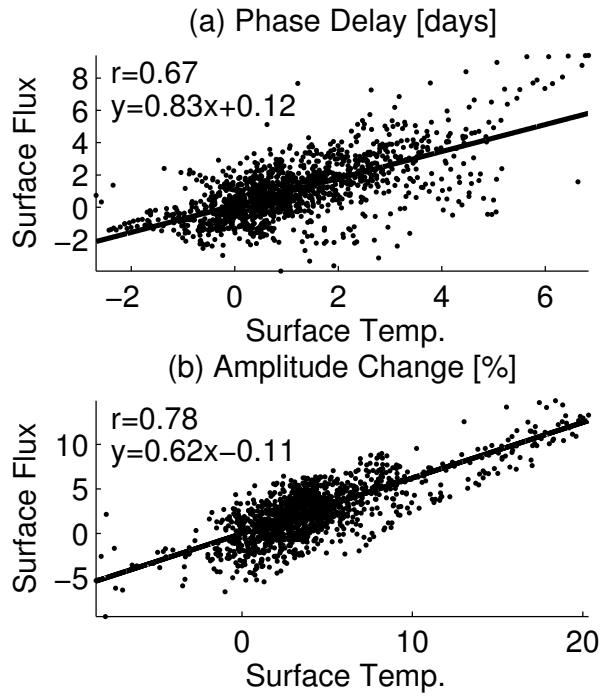


FIG. 14. Scatter plot of 21st century seasonality changes of surface flux versus surface temperature for (a) phase and (b) amplitude for subtropical ocean grid boxes. There is an area-weighted correlation between these two variables for both phase and amplitude, indicating that, for example, subtropical locations that have large surface flux delays tend to have large surface temperature delays. The data is restricted to 15° – 30° in both hemispheres and does not include locations where the annual harmonic of each variable does not dominate its total variance. The solid line represents the area-weighted least-squares regression.